University of Groningen

Spurious multiple equilibria introduced by convective adjustment

Toom, Matthijs den; Dijkstra, Henk A.; Wubs, Friederik

Published in:
Ocean modelling

DOI:
10.1016/j.ocemod.2011.02.009

IMPORTANT NOTE: You are advised to consult the publisher's version (publisher's PDF) if you wish to cite from it. Please check the document version below.

Document Version
Publisher's PDF, also known as Version of record

Publication date:
2011

Link to publication in University of Groningen/UMCG research database

Citation for published version (APA):
Toom, M. D., Dijkstra, H. A., & Wubs, F. W. (2011). Spurious multiple equilibria introduced by convective adjustment. Ocean modelling, 38(1-2), 126-137. DOI: 10.1016/j.ocemod.2011.02.009

Copyright
Other than for strictly personal use, it is not permitted to download or to forward/distribute the text or part of it without the consent of the author(s) and/or copyright holder(s), unless the work is under an open content license (like Creative Commons).

Take-down policy
If you believe that this document breaches copyright please contact us providing details, and we will remove access to the work immediately and investigate your claim.

Downloaded from the University of Groningen/UMCG research database (Pure): http://www.rug.nl/research/portal. For technical reasons the number of authors shown on this cover page is limited to 10 maximum.

Download date: 10-02-2018

Ocean Modelling 38 (2011) 126–137

Contents lists available at ScienceDirect

Ocean Modelling

journal homepage: www.elsevier.com/locate/ocemod

Spurious multiple equilibria introduced by convective adjustment

Matthijs den Toom [a,*], Henk A. Dijkstra [a], Fred W. Wubs [b]

[a] Institute for Marine and Atmospheric Research Utrecht, Department of Physics and Astronomy, Utrecht University, Utrecht, The Netherlands
[b] Department of Mathematics and Computer Science, University of Groningen, Groningen, The Netherlands

ARTICLE INFO

Article history:
Received 6 October 2010
Received in revised form 27 January 2011
Accepted 22 February 2011
Available online 1 March 2011

Keywords:
Convection
Parameterisation
Bifurcation analysis

ABSTRACT

The application of bifurcation analysis to ocean climate models is substantially hampered by difficulties associated with the use of convective adjustment, i.e. a parameterisation of convection in which the vertical diffusion of heat and salt is greatly enhanced whenever the water column becomes statically unstable. When tracking steady solutions of these models in parameter space, problems arise due to the occurrence of a multitude of saddle-node bifurcations, each of which is related to a minor reorganisation of convection. In this paper, we analyse the origin of the multiple steady states in detail using a one-dimensional column model. By analytical evaluation of the eigenvalue problem conditions are formulated under which bifurcations may occur. Using numerical continuation methods a regime of multistability is identified and it is shown that the number of coexisting steady states increases with increasing resolution, while the extent of parameter space in which they occur decreases. A comparison of the numerical results to corresponding analytical solutions reveals that the multiple equilibria are inherent to the discretisation and hence artificial. Apparently, successful application of convective adjustment requires knowledge of subgrid-scale tracer fields. Two alternative convective adjustment schemes are proposed that (partially) overcome these problems. Results from a fully implicit model based on the two-dimensional primitive equations indicate that the physically relevant phenomena due to the nonlinear character of large-scale oceanic flow, notably the bifurcations related to the salt advection feedback, are preserved under the alternative formulations.

© 2011 Elsevier Ltd. All rights reserved.

1. Introduction

The possibility of a rapid reduction in strength of the Atlantic meridional overturning circulation (MOC) as a consequence of anthropogenic greenhouse forcing represents a crucial uncertainty in predicting the future climate (Meehl et al., 2007). Although some palaeo-climatological data suggest that the last glacial period witnessed a series of major reorganisations of the Atlantic circulation (Clark et al., 2002), only with models one can assess if these are an intrinsic property of the climate system. To do so, these models need to adequately capture the relevant non-linear behaviour of the ocean circulation. In the present work we demonstrate the difficulty of faithfully representing the effect of the small-scale non-linear process of convection in models that simulate the (Atlantic) MOC.

One of the main reasons that the ocean's dynamics are not linear, is the fact that flow strengths are in part determined by the density field, while this, in turn, is affected by advective processes. Even if the non-linearity of the equation of state is ignored, temperature and salinity have different roles in this two-way interaction. Because the surface heat flux depends on surface temperature, while there is no such negative feedback in case of salinity, the MOC is more sensitive to perturbations of salinity than of temperature. This corollary forms the basis of the two major positive feedbacks that have been proposed to have an effect on the large-scale circulation: the *con*vective and the *ad*vective feedback (Rahmstorf, 1999).

The convective feedback has been studied by Welander (1982) and Lenderink and Haarsma (1994) using a simple box model, consisting of a surface box that is in contact with the atmosphere, and a box representing the deep ocean, where temperature and salinity are fixed. They parameterised the effect of convection by a diffusive exchange of water properties, using a diffusivity that is small when the water in the upper box is less dense than that in the deep box, but takes a very large value in convective conditions. Welander (1982) demonstrated that the model may show spontaneous oscillations due to the system switching between convective and non-convective conditions before reaching either of the corresponding fixed points. The analysis of Lenderink and Haarsma (1994) showed that there also exist parameter regimes where the convective and the non-convective state co-exist as stable steady states. Unfortunately, we are not aware of studies that examine the relevance of the convective feedback mechanism in models that resolve the convective dynamics, nor of supporting observations.

* Corresponding author. Tel.: +31 30 253 7759.
E-mail address: m.dentoom@uu.nl (M. den Toom).

1463-5003/$ - see front matter © 2011 Elsevier Ltd. All rights reserved.
doi:10.1016/j.ocemod.2011.02.009

The seminal reference on the advective feedback is by Stommel (1961). Using a box model he showed that under certain conditions multiple stable steady states coexist, corresponding to different flow patterns. In one state the circulation is driven by an imposed thermal gradient, while the other state is characterised by an opposite circulation driven by a salinity gradient that is sustained by the flow itself. Multiple equilibria due to the advective feedback have also been found in more complete models of the ocean circulation, such as two-dimensional (latitude/depth) models (Vellinga, 1997), three-dimensional ocean-only models (Marotzke and Willebrand, 1991) and models of intermediate complexity (EMICS, Rahmstorf et al., 2005). Whether the existence of bistability transfers to the full climate system is still subject of active research. Currently, the lack of computational resources prevents this issue from being addressed with state-of-the-art climate models.

A particularly insightful way to study feedbacks in ocean models is the application of numerical bifurcation analysis (Dijkstra and Ghil, 2005). Using special techniques (Seydel, 1988), it is possible to follow branches of steady states in parameter space and evaluate the linear stability of those states. These methods thus allow for a more systematic investigation of the origin of multiplicity and intrinsic variability than would be possible with traditional time stepping. When this approach is used to study the salt advection feedback, however, its effectiveness is severely limited due to the parameterisation of convection.

Oceanic convection can only be resolved numerically if a very fine horizontal resolution (<1 km) is employed (Jones and Marshall, 1993), which is not (yet) possible in models that are used to study large-scale dynamics. Without a parameterisation of convection, such models may admit solutions in which statically unstable density stratification prevails, and associated flow patterns are unrealistic (Marotzke and Scott, 1999). One of the simplest remedies is to implement a scheme that causes strong vertical mixing of temperature and salinity when the stratification across an interface is unstable. This method is called *convective adjustment* (CA) and is in fact very similar to the inter-box exchange in the box model of Welander (1982) and Lenderink and Haarsma (1994). In conventional time-marching codes two different approaches are used (Marotzke, 1991): (1) complete removal of static instabilities at the end of each time step in an iterative procedure; and (2) reduction of positive density gradients by greatly enhanced vertical diffusion. Since our interest is in numerical bifurcation analysis, for which the model equations need to be continuous in time, we focus on the second method. It should be noted, though, that the first approach can be thought of as a limit case of the second, in which the convective diffusivity tends to infinity (Schmidt and Mysak, 1996).

Convective adjustment is known to have serious deficiencies. To begin with, Hughes et al. (2009) noted that it disrupts the coupling between the evolution of basin integrated kinetic and potential energy. In addition, it falsely reduces the available potentially energy production from the surface buoyancy flux. Even if consistent energy fluxes are not required, CA may give rise to artificial model behaviour due to the strong vertical coupling between grid points it implies. Cessi (1996) and Cessi and Young (1996) investigated the interaction of CA and horizontal diffusion by coupling an array of boxes similar to the "flip-flop" model of Welander (1982). They demonstrated analytically that when mixing is applied instantaneously, the scheme leads to the spontaneous emergence of the smallest resolved horizontal scale. Numerical simulations may not reveal this grid-scale instability, though, because of errors due to the finite size of the time step, or roundoff. Yet, it was suggested that these problems may be avoided when the convective diffusivity is finite and smaller than some critical value (Cessi, 1996; Cessi and Young, 1996).

Even so, there appears to be yet another deficiency of the CA method, which is less easily perceived when using the conventional time-stepping approach. In determining bifurcation diagrams of zonally averaged ocean models using continuation methods, Vellinga (1997, Chapter 4) found a multitude of saddle-node bifurcations, despite the use of a moderate intensity of convection (corresponding to a timescale of convective mixing of about 3 yr). The bifurcations were absent in the model without CA. In a further investigation of their origin, Vellinga (1998, hereafter "V98") used a one-dimensional column model with only temperature as tracer to study the behaviour of CA in isolation. He concluded that the regular occurrence of saddle-node bifurcations does not reflect a real physical process but is caused by the way in which convection is treated in ocean models. His results thus provide a warning that convective adjustment is responsible for spurious equilibria. In practice, the saddle-node bifurcations due to CA are so numerous that the effectiveness of numerical continuation methods is severely compromised, which motivates to reexamine the problem. We want to stress, though, that the peculiarities of CA discussed in this paper are not unique to the steady state modelling approach, but also apply to time-stepping methods.

In the present work we extend the preliminary analysis of V98 regarding the one-dimensional column model by including both temperature and salt. Numerical results, in conjunction with an analytical examination of the linear stability of steady states, demonstrate that the convective feedback (Welander, 1982; Lenderink and Haarsma, 1994) operates on the grid scale. In addition, we provide analytical solutions of the model and compare them to corresponding numerical results, which allows us to firmly establish the artificial nature of the multiple equilibria associated with CA. Finally, we propose alternative formulations to eliminate, or at least reduce, their occurrence.

In Section 2, we show the effect of CA on the equilibria of a two-dimensional primitive equation model. The analysis of the one-dimensional column model is presented in Section 3 and the alternative CA schemes in Section 4. A summary and discussion follows in Section 5.

2. Spurious multiple equilibria in a two-dimensional ocean model

In this section, we aim to illustrate the problem of spurious multiple equilibria due to CA in a model that captures the salt advection feedback (Stommel, 1961). We therefore consider a two-dimensional (latitude/depth) configuration. Compared to the full three-dimensional case, it is much more tractable numerically, because the number of unknowns that must be solved for is typically one order of magnitude smaller. The model we use here is equivalent to the one analysed for the case of no CA in section 3a of the paper by Weijer and Dijkstra (2001), and is very similar to the model studied by V98. We choose this particular model, because results presented in the subsequent sections of Weijer and Dijkstra (2001) demonstrate a close qualitative similarity between the bifurcation structure of two- and three-dimensional flows.

The experiments with the two-dimensional model are conducted with the B-grid version of the ThermoHaline Circulation Model (THCM, De Niet et al., 2007), which is a fully-implicit ocean-only model based on the hydrostatic primitive equations in spherical coordinates. It employs a pseudo-arclength continuation technique (Keller, 1977) to calculate branches of steady states, and uses the Newton–Raphson method to converge to individual solutions. In addition, the model implements the Jacobi–Davidson QZ method (Sleijpen and Van der Vorst, 1996) to solve eigenvalue problems. The large linear systems that arise from these techniques are solved iteratively using a tailored preconditioner, which is described in detail by De Niet et al. (2007).

Table 1
Fixed model parameters of the two-dimensional ocean model.

$D = 4.0 \times 10^3$ m	$H_m = 2.5 \times 10^2$ m
$\phi_N = 60°$	$\rho_0 = 1.0 \times 10^3$ kg m^{-3}
$r_0 = 6.371 \times 10^6$ m	$T_0 = 15.0$ °C
$g = 9.8$ m s^{-2}	$S_0 = 35.0$ psu
$A_H = 2.2 \times 10^{12}$ m^2 s^{-1}	$\alpha_T = 1.0 \times 10^{-4}$ K^{-1}
$A_V = 1.0 \times 10^{-3}$ m^2 s^{-1}	$\alpha_S = 7.6 \times 10^{-4}$ psu^{-1}
$K_H = 1.0 \times 10^3$ m^2 s^{-1}	$\epsilon = 2.0 \times 10^3$
$K_V = 1.0 \times 10^{-4}$ m^2 s^{-1}	$\tau = 75.0$ days

2.1. Formulation

There are two active tracers: temperature T_* (stars indicate dimensional quantities) and salinity S_*, which are related to the density ρ_* by a linear equation of state

$$\rho_* = \rho_0(1 - \alpha_T(T_* - T_0) + \alpha_S(S_* - S_0)), \tag{1}$$

where α_T and α_S are the thermal expansion and haline contraction coefficients, respectively, and ρ_0, T_0, and S_0 are reference quantities. The numerical values of these (and following) fixed model parameters are summarised in Table 1.

In order to eliminate longitudinal dependence from the problem, we consider a purely buoyancy-driven flow on a non-rotating Earth and prescribe free-slip conditions at the lateral boundaries (which avoids the necessity of boundary layer formation). We furthermore assume that inertia can be neglected in the meridional momentum equation. The mixing of momentum and tracers due to eddies is parameterised by simple anisotropic diffusion. The equations for the meridional velocity v_*, vertical velocity w_*, pressure p_*, and the tracers T_* and S_* are thus given by

$$0 = -\frac{1}{\rho_0 r_0}\frac{\partial p_*}{\partial \phi} + A_V\frac{\partial^2 v_*}{\partial z_*^2} + \frac{A_H}{r_0^2}\left(\frac{1}{\cos\phi}\frac{\partial}{\partial\phi}\left(\cos\phi\frac{\partial v_*}{\partial\phi}\right) + (1-\tan^2\phi)v_*\right), \tag{2a}$$

$$0 = -\frac{1}{\rho_0}\frac{\partial p_*}{\partial z_*} + g(\alpha_T T_* - \alpha_S S_*), \tag{2b}$$

$$0 = \frac{1}{r_0\cos\phi}\frac{\partial v_*\cos\phi}{\partial\phi} + \frac{\partial w_*}{\partial z_*}, \tag{2c}$$

$$\frac{\partial T_*}{\partial t_*} + \frac{v_*}{r_0}\frac{\partial T_*}{\partial\phi} + w_*\frac{\partial T_*}{\partial z_*} = \frac{K_H}{r_0^2\cos\phi}\frac{\partial}{\partial\phi}\left(\cos\phi\frac{\partial T_*}{\partial\phi}\right) + K_V\frac{\partial^2 T_*}{\partial z_*^2} + \mathrm{CA}(T_*), \tag{2d}$$

$$\frac{\partial S_*}{\partial t_*} + \frac{v_*}{r_0}\frac{\partial S_*}{\partial\phi} + w_*\frac{\partial S_*}{\partial z_*} = \frac{K_H}{r_0^2\cos\phi}\frac{\partial}{\partial\phi}\left(\cos\phi\frac{\partial S_*}{\partial\phi}\right) + K_V\frac{\partial^2 S_*}{\partial z_*^2} + \mathrm{CA}(S_*). \tag{2e}$$

Here, t_* is time, ϕ latitude, z_* the vertical coordinate, r_0 the radius of Earth, g the acceleration due to gravity, A_H (A_V) the horizontal (vertical) eddy viscosity, and K_H (K_V) the horizontal (vertical) eddy diffusivity. The term CA represents convective adjustment.

The equations are solved on an equatorially symmetric, flat-bottomed domain. The basin is bounded by latitudes $\phi = -\phi_N$ and $\phi = \phi_N$ and has depth D. In order to calculate transports, we assume it has a width of 64°. The resolution is 3.75° in the horizontal and 250 m in the vertical. Free-slip conditions apply at the lateral walls and at the bottom. Rigid lid conditions are assumed at the surface and atmospheric pressure is neglected. The wind stress is zero everywhere, and "mixed" boundary conditions apply for temperature and salinity,

$$K_V\frac{\partial T_*}{\partial z_*} = \frac{H_m}{\tau}(\widetilde{T}(\phi) - T_*) \quad \widetilde{T}(\phi) = 10.0\cos(\pi\phi/\phi_N), \tag{3a}$$

$$K_V\frac{\partial S_*}{\partial z_*} = S_0\widetilde{Q}(\phi) \quad \widetilde{Q}(\phi) = \gamma\frac{\cos(\pi\phi/\phi_N)}{\cos(\phi)}. \tag{3b}$$

This formulation implies that temperatures in the upper model layer (of depth H_m) are relaxed to a prescribed profile $\widetilde{T}$ at a rate τ^{-1}, while salinity is forced by a net freshwater flux $\widetilde{Q}$, which is converted to an equivalent virtual salinity flux by multiplication with S_0. Although in a crude way, these equations express that ocean–atmosphere interaction affects temperature and salinity in a fundamentally different way. In the next subsection we present the results of sensitivity experiments, in which the amplitude of the freshwater forcing γ is the control parameter.

The introduction of CA is the only change to the model analysed in Section 3a of the paper by Weijer and Dijkstra (2001). It acts solely on the tracers and is implemented as enhanced diffusion, which for a tracer C_* takes the form

$$\mathrm{CA}(C_*) = K_V F_0\frac{\partial}{\partial z_*}\left(\mathcal{F}\left(\frac{D}{\rho_0}\frac{\partial\rho_*}{\partial z_*}\right)\frac{\partial C_*}{\partial z_*}\right). \tag{4}$$

Here, F_0 is the efficiency of convection and $\mathcal{F}$ is a continuous approximation of the Heaviside step function (see Fig. 3),

$$\mathcal{F}(x) = \max(0, \tanh[(\epsilon x)^3]). \tag{5}$$

The steepness of the transition from 0 to 1 is determined by the selectivity ϵ; in the limit $\epsilon \to \infty$ the function $\mathcal{F}$ tends to the step function. The actual value of ϵ is determined from experience. The use of a smooth function is required for the application of numerical bifurcation analysis, but the choice of which function is obviously not unique. We return to this issue in Section 3.2, where we show that the shape of the function can influence the dynamical behaviour of the model.

2.2. Results

We start with a brief recapitulation of the case without CA ($F_0 = 0$); a more extensive analysis is given in Weijer and Dijkstra (2001). The main characteristic of the model is that, as a result of the salt advection feedback (Stommel, 1961), there is a parameter regime in which equatorially asymmetric solutions exist despite the symmetry imposed by the geometry and forcing. The complex dynamical behaviour of the model is best illustrated by the bifurcation diagram in Fig. 1a. For each value of the freshwater forcing strength γ there is a single equatorially symmetric solution, which is characterised by surface flow away from (towards) the equator for $\gamma \leqslant (\geqslant) 0.17$ m yr^{-1}. The symmetric state is linearly stable, except for the part of the branch between the two pitchfork bifurcations at $\gamma = 0.04$ m yr^{-1} and $\gamma = 0.35$ m yr^{-1}. The pitchfork bifurcations also connect two branches of equatorially asymmetric solutions. Each of these is linearly stable between the first pitchfork at $\gamma = 0.04$ m yr^{-1} and the Hopf bifurcation at $\gamma = 0.44$ m yr^{-1}. At $\gamma = 0.46$ m yr^{-1} linear stability changes again due to a saddle-node bifurcation. For a given γ the solution on one branch is the mirror image of the solution on the other branch. An example of an asymmetric solution with northward surface flow across the equator is shown in Fig. 1b. Evidently, the density stratification is statically unstable in a significant portion of the domain north of about 20°N.

If we start from the solution in Fig. 1b and increase the convective efficiency to $F_0 = 10^2$, the result is the solution shown in Fig. 2b. As expected, the application of CA reduces positive density gradients. The consequences are: (a) steeper isopycnals in the northern part of the domain, (b) increased bottom density, (c) stronger stratification to the south of the overturning maximum, and (d) a more vigorous meridional overturning circulation. The bifurcation diagram (Fig. 2a) shows that the dynamical behaviour of the model is also changed due to the addition of CA. Although the overall structure is similar compared to the case without CA, a large number of additional saddle-node bifurcations has appeared, which, in the following section, will be shown to be artificial. The spurious

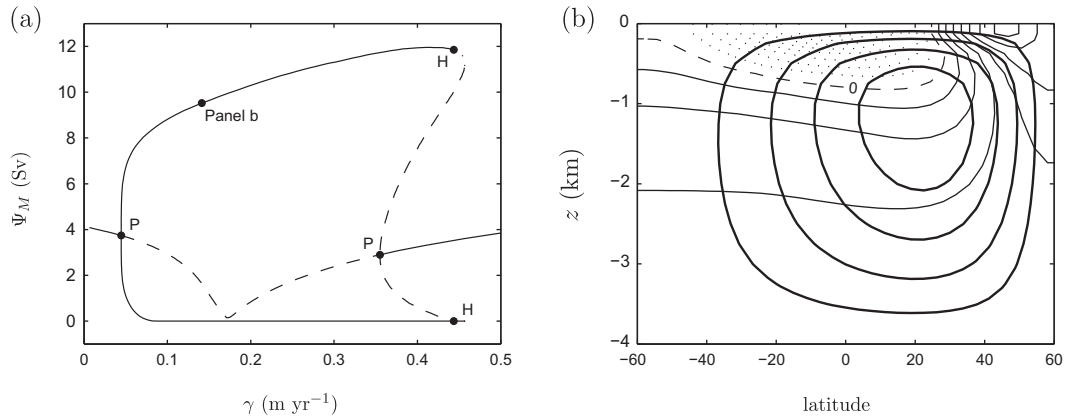

Fig. 1. (a) Bifurcation diagram for the two-dimensional model without convective adjustment, using the freshwater forcing strength γ as control parameter. The plot shows the maximum of the meridional overturning streamfunction Ψ_M in Sverdrups (1 Sv = 10^6 m^3 s^{-1}). Branches drawn as solid lines represent solutions that are linearly stable; dashed (dotted) lines indicate that one (two) of the eigenvalues is (are) positive. Pitchfork (P) and Hopf (H) bifurcations are marked in the diagram. (b) Meridional stream function (thick lines) and density relative to ρ_0 for the solution indicated in (a) by "panel b". Contour interval is 2 Sv and 0.1 kg m^{-3}, respectively.

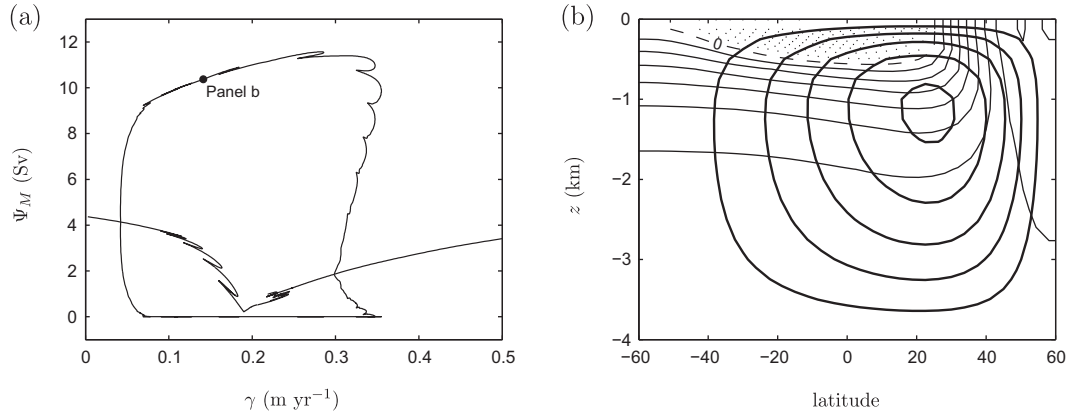

Fig. 2. (a) Bifurcation diagram for the two-dimensional model with traditional convective adjustment and $F_0 = 10^2$. The linear stability of the steady states is not indicated. (b) Same as Fig. 1b.

saddle-node bifurcations define relatively narrow regions in parameter space where multiple steady states are present. Since our focus is on artificial multiple equilibria we have not calculated the linear stability of the steady states, which would have been very computationally expensive. The results of V98, however, show that apart from spurious saddle-node bifurcations, CA is also associated with complex intrinsic variability through the occurrence of numerous additional Hopf bifurcations.

3. Analysis

It is clear from the previous section that CA has a peculiar effect on the dynamics of simulated ocean flow, but the two-dimensional model is too complex to analyse the problem. We therefore turn to the one-dimensional column model introduced by V98, but instead of considering only temperature, we extend it to include salinity.

3.1. Formulation of the one-dimensional model

The model consists of a column with depth D. On this domain we solve the vertical diffusion equation for the active tracers temperature and salinity:

$$\frac{\partial T_*}{\partial t_*} = K_V \frac{\partial}{\partial z_*}\left([1 + F_0 \mathcal{K}_{T_*}]\frac{\partial T_*}{\partial z_*}\right) - \kappa\left(i_T^{\text{res}} T_* - \widetilde{T}_*(z_*)\right), \tag{6a}$$

$$\frac{\partial S_*}{\partial t_*} = K_V \frac{\partial}{\partial z_*}\left([1 + F_0 \mathcal{K}_{S_*}]\frac{\partial S_*}{\partial z_*}\right) - \kappa\left(i_S^{\text{res}} S_* - \widetilde{S}_*(z_*)\right). \tag{6b}$$

At the surface ($z_* = 0$) and the bottom ($z_* = -D$) no-flux conditions apply. The functions $\mathcal{K}_T$ and $\mathcal{K}_S$ will be referred to as convective adjustment functions, whose form may differ between the cases considered. The forcing of the system is given by the rightmost term. For $i^{\text{res}} = 1$ it acts to relax the tracer to a prescribed profile at a rate κ, whereas for $i^{\text{res}} = 0$ it represents a fixed source of heat/salt. The density is computed from the linear equation of state given in Eq. (1).

The system in Eq. (6) is nondimensionalised by making the following substitutions:

$$t = \kappa t_*, \quad z = D^{-1} z_*,$$
$$T = \alpha_T (T_* - T_0), \quad S = \alpha_S (S_* - S_0),$$

which gives

$$\frac{\partial T}{\partial t} = \frac{1}{P}\frac{\partial}{\partial z}\left([1 + F_0 \mathcal{K}_T]\frac{\partial T}{\partial z}\right) - \left(i_T^{\text{res}} T - \widetilde{T}(z)\right), \tag{7a}$$

$$\frac{\partial S}{\partial t} = \frac{1}{P}\frac{\partial}{\partial z}\left([1 + F_0 \mathcal{K}_S]\frac{\partial S}{\partial z}\right) - \left(i_S^{\text{res}} S - \widetilde{S}(z)\right). \tag{7b}$$

Here, $P = \frac{D^2 \kappa}{K_V}$, which may be interpreted as the vertical Péclet number if $i^{\text{res}} = 1$. With D and K_V as in Table 1 and $\kappa^{-1} \approx 5$ yr, we get $P \equiv 10^3$. This value will be used throughout and corresponds to the "strong restoring" case considered by V98.

We use the same temperature forcing as V98,

$$\widetilde{T}(z) = \cos(2\pi z), \tag{8}$$

which is such that it tends to stabilise (destabilise) the stratification above (below) $z = -0.5$. The salinity forcing is given by

$$\widetilde{S}(z) = \gamma \cos(\pi z). \tag{9}$$

As in the experiments with the two-dimensional model the salinity forcing strength γ is the control parameter for the sensitivity analysis presented in the next subsections. For negative (positive) γ the salinity forcing acts to stabilise (destabilise) the stratification in the entire column. So, by varying γ we can change the stratification. In addition, we may compare the behaviour of CA in cases in which temperature and salinity gradients have an opposite effect on the density gradient to cases in which the effect is of the same sign.

In this section we consider convective adjustment functions ($\mathcal{K}$) that only depend on the density gradient. It is therefore useful to reformulate Eqs. (7a) and (7b) in terms of density. The nondimensional form of the equation of state [Eq. (1)] is given by

$$\rho = \rho_0^{-1}(\rho_* - \rho_0) = S - T. \tag{10}$$

Because there are two independent variables in the original system (T and S), a complete description of the density evolution requires the definition of a complementary variable. It is convenient to use a quantity that is completely independent of density; we therefore define

$$\mu = S + T, \tag{11}$$

which is commonly referred to as "spiciness", being largest for hot and salty water (Flament, 2002). Obviously, a water mass characterised by a certain temperature and salinity may equivalently be described in terms of its density and spiciness. In a T versus S diagram the isolines of ρ and μ would appear as a set of perpendicular lines, tilted at a 45 degree angle with respect to the axes. Combining Eqs. (7a) and (7b) now gives the following alternative formulation of the problem:

$$\frac{\partial \rho}{\partial t} = \frac{1}{P}\frac{\partial}{\partial z}\left(\left[1 + F_0 \mathcal{K}_\rho\right]\frac{\partial \rho}{\partial z}\right) - \left(i_+^{\mathrm{res}}\rho + i_-^{\mathrm{res}}\mu - \tilde{\rho}(z)\right), \tag{12a}$$

$$\frac{\partial \mu}{\partial t} = \frac{1}{P}\frac{\partial}{\partial z}\left(\left[1 + F_0 \mathcal{K}_\mu\right]\frac{\partial \mu}{\partial z}\right) - \left(i_-^{\mathrm{res}}\rho + i_+^{\mathrm{res}}\mu - \tilde{\mu}(z)\right), \tag{12b}$$

where

$$i_+^{\mathrm{res}} = \frac{i_S^{\mathrm{res}} + i_T^{\mathrm{res}}}{2}, i_-^{\mathrm{res}} = \frac{i_S^{\mathrm{res}} - i_T^{\mathrm{res}}}{2},$$

and $\tilde{\rho}(z) = \widetilde{S}(z) - \widetilde{T}(z)$, $\tilde{\mu}(z) = \widetilde{S}(z) + \widetilde{T}(z)$. The coordinate transformation applied here also has other applications in oceanography. For example, it offers a meaningful way to examine the ubiquitous phenomenon of density compensation, which refers to the situation where temperature and salinity compensate in their effects on density. In that case all spatial thermohaline variability is projected onto spiciness.

3.2. The choice of convective adjustment function

Before turning to the problem of how CA introduces spurious additional multiple equilibria as in the results of Section 2, we show why the analysis of the column model by V98 is incomplete. We therefore focus on the influence that the choice of convective adjustment function has on the model dynamics. The occurrence of bifurcations is associated with zero eigenvalues (λ) of the Jacobian matrix, which results from linearising the model around a steady state. Hence, a central element in the analysis below is the evaluation of criteria under which zero eigenvalues can exist. In the following $\partial_z X$ means $\partial X/\partial z$.

As in V98 we consider a single active tracer (density). We therefore take $i_-^{\mathrm{res}} = 0$, which means that temperature and salinity are either both relaxed towards a prescribed profile ($i_T^{\mathrm{res}} = i_S^{\mathrm{res}} = 1$), or both forced by a fixed source ($i_T^{\mathrm{res}} = i_S^{\mathrm{res}} = 0$). In both cases spiciness does not influence density, but rather adjusts passively to changes in the diffusivity implied by changes in density. Furthermore, again following V98, we define the convective adjustment functions as $\mathcal{K}_\rho = \mathcal{K}_\mu = \mathcal{G}(\partial_z \rho)$ with

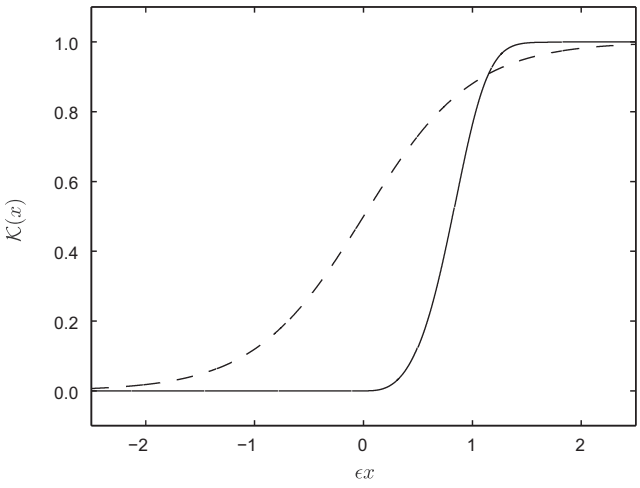

Fig. 3. Convective adjustment functions $\mathcal{F}(x)$ (drawn) and $\mathcal{G}(x)$ (dashed).

$$\mathcal{G}(x) = \frac{1}{2}(1 + \tanh(\epsilon x)). \tag{13}$$

The function $\mathcal{G}$ will be contrasted with the function $\mathcal{F}$ introduced in Eq. (5). As illustrated in Fig. 3 the most obvious difference between the two functions is $\mathcal{F}$ being zero for negative x, while $\mathcal{G}$ is not.

We first assume Eq. (12a) has a certain steady solution $\bar{\rho}$, and analyse what behaviour can be expected if it is slightly perturbed: $\rho = \bar{\rho} + \Delta\rho$. After linearisation and substitution of solutions proportional to $e^{\lambda t}$ the following eigenvalue equation is found:

$$\lambda \Delta\rho = \frac{1}{P}\frac{\partial}{\partial z}\left(\left[1 + F_0\overline{\mathcal{G}} + F_0\overline{\mathcal{G}}'\frac{\partial \bar{\rho}}{\partial z}\right]\frac{\partial \Delta\rho}{\partial z}\right) - i_+^{\mathrm{res}}\Delta\rho, \tag{14}$$

where $\overline{\mathcal{G}} = \mathcal{G}(\partial_z \bar{\rho})$ and the prime indicates differentiation. Next, we investigate whether the linear self-adjoint operator, implicitly defined in the right-hand side, is negative definite in the inner product

$$\int_{-1}^{0} \widehat{f} g \, dz$$

on a space of functions (f,g,...) for which the vertical derivative at bottom and top is zero ($\widehat{f}$ is the complex conjugate of f). The latter is equivalent to the statement that all eigenvalues of the operator are negative on the mentioned function space. Multiplying Eq. (14) by $\widehat{\Delta\rho}$ and integrating from $z = -1$ to $z = 0$ yields

$$\frac{1}{P}\int_{-1}^{0}\left(\left[1 + F_0\overline{\mathcal{G}} + F_0\overline{\mathcal{G}}'\frac{\partial \bar{\rho}}{\partial z}\right]\frac{\partial \widehat{\Delta\rho}}{\partial z}\frac{\partial \Delta\rho}{\partial z}\right)dz$$
$$= -\left(i_+^{\mathrm{res}} + \lambda\right)\int_{-1}^{0}|\Delta\rho|^2 dz, \tag{15}$$

where we have used that $\partial_z \Delta\rho = 0$ at bottom and top.

Now suppose that

$$\Gamma_\rho^\rho \equiv \left[1 + F_0\overline{\mathcal{G}} + F_0\overline{\mathcal{G}}'\frac{\partial \bar{\rho}}{\partial z}\right] \geqslant 0 \quad \forall z \in [-1, 0], \tag{16}$$

and, additionally, that $i_+^{\mathrm{res}} = 1$ (relaxation of T and S). In that case Eq. (15) implies that the eigenvalues satisfy $\lambda \leqslant -1$, meaning that the steady state $\bar{\rho}$ is linearly stable. If instead $i_+^{\mathrm{res}} = 0$ (fixed flux), density is only determined up to a constant, which results in a zero eigenvalue. This singularity is easily removed by imposing an additional integral constraint on both T and S.

So, for eigenfunctions with nonnegative eigenvalues to exist, it is required that $\Gamma^{\rho}_{\rho} < 0$ for some range of z. The only term in Γ^{ρ}_{ρ} that can be negative is $\overline{\mathcal{G}}'\partial_z\bar{\rho}$. In fact, it is negative when the stratification is stable, since $\mathcal{G}$ is a monotone increasing function (Fig. 3) and hence $\overline{\mathcal{G}}'$ is always positive. Bifurcation points in this model are thus related to the following feedback: If at a certain point the stratification becomes weak, but remains statically stable, vertical diffusion is enhanced; this causes stratification to become weaker, which, in turn, results in even stronger vertical diffusion. It should be stressed that this mechanism is different from the convective feedback (Welander, 1982; Lenderink and Haarsma, 1994) discussed in the introduction. It does not depend on the presence of two active tracers (T and S), but rather is inherent to the shape of $\mathcal{G}$. In the following it will be referred to as "self-sustaining diffusion".

An analytical steady state solution of Eq. (12a) with $\mathcal{K} = \mathcal{G}$ is not available, so the "true" expression of the self-sustaining diffusion feedback is unknown. Therefore we turn to the discrete problem. We consider a discretisation in which numerical solutions are calculated on an l-point equidistant grid, and derivatives are approximated by central differences. Repeating the steps that lead to Eq. (15), but now defining the inner product as a summation, leads to

$$\frac{l^2}{\overline{P}}\sum_{k=1}^{l-1}\left(\left[1+F_0\overline{\mathcal{G}}_+ + F_0\overline{\mathcal{G}}'_+ l(\bar{\rho}_{k+1}-\bar{\rho}_k)\right]\cdot\left|\Delta\rho_{k+1}-\Delta\rho_k\right|^2\right) = -\left(i^{\mathrm{res}}_+ + \lambda\right)\sum_{k=1}^{l}|\Delta\rho_k|^2, \tag{17}$$

where ρ_k is the density at level $k \in \{1,\ldots,l\}$, and

$$\overline{\mathcal{G}}_+ = \mathcal{G}(l[\bar{\rho}_{k+1}-\bar{\rho}_k]).$$

Comparison of Eqs. (15) and (17) shows that the latter may also be obtained directly from the former by replacing integrals with sums and discretising the derivatives. The feedback of self-sustaining diffusion is hence also present in the discrete model and, indeed, explains the occurrence of saddle-node bifurcations and multiple steady states in the one-dimensional model of V98 (his Figs. 11 and 12).

Yet, closer examination of Eq. (17) suggests that the stability properties of the discrete system may be different from the continuous system, and possibly depend on l. Even if the set $\bar{\rho}_k$ for $k = 1,\ldots,l$ closely resembled the (unknown) true solution at the levels of discretisation, the result of the strongly non-linear operator $\overline{\mathcal{G}}_+$ would depend on the resolution. Furthermore, the diffusion feedback may only operate at the level of the interfaces determined by the discretisation. These notions form a provisional explanation for the observation of V98 that the multiplicity of steady states in a given parameter space depends on resolution.

When we contrast the function $\mathcal{G}$ with the function $\mathcal{F}$ [Eq. (5)] it is clear, though, that this analysis is not complete. Because $\overline{\mathcal{F}}'\partial_z\bar{\rho}$ is always nonnegative, using the latter function would eliminate the self-sustaining diffusion feedback. As a result, there would be no bifurcations (we have confirmed this for the discrete case). So, for $i^{\mathrm{res}}_- = 0$ and using $\mathcal{F}$, we can prove that no unfavourable feedback can occur in the discrete system, where it can if we use $\mathcal{G}$. Nevertheless, we observe spurious multiple equilibria in the two-dimensional model computations using $\mathcal{F}$ (Fig. 2). The conclusion is therefore that it is not sufficient to consider only the case of a single active tracer ($i^{\mathrm{res}}_- = 0$); we also have to consider the case with interaction between density and spiciness in order to understand the two-dimensional model results.

3.3. Mixed forcing

We examine the case of "mixed forcing" by taking ($i^{\mathrm{res}}_- \neq 0$). Furthermore, let $\mathcal{K}_\rho = \mathcal{K}_\mu = \mathcal{F}(\partial_z\rho)$. In the eigenvalue analysis we now need to include both the equations for density and spiciness and arrive at

$$\int_{-1}^{0}\left[\frac{\Phi^{\rho}_{\rho}}{P}\frac{\partial\widehat{\Delta\rho}}{\partial z}\frac{\partial\Delta\rho}{\partial z}+\frac{\Phi^{\mu}_{\mu}}{P}\frac{\partial\widehat{\Delta\mu}}{\partial z}\frac{\partial\Delta\mu}{\partial z}+2i^{\mathrm{res}}_T|\Delta T|^2+2i^{\mathrm{res}}_S|\Delta S|^2\right]\mathrm{d}z = -\int_{-1}^{0}\left[\frac{\Phi^{\mu}_{\rho}}{P}\frac{\partial\widehat{\Delta\mu}}{\partial z}\frac{\partial\Delta\rho}{\partial z}+\lambda\left(|\Delta\rho|^2+|\Delta\mu|^2\right)\right]\mathrm{d}z, \tag{18}$$

where we used the following short-hand notations:

$$\Phi^{\rho}_{\rho} - 1 = F_0\overline{\mathcal{K}}_\rho + F_0\bar{\mathcal{K}}_\rho{}'\frac{\partial\bar{\rho}}{\partial z} = F_0\overline{\mathcal{F}} + F_0\overline{\mathcal{F}}'\frac{\partial\bar{\rho}}{\partial z}, \tag{19a}$$

$$\Phi^{\mu}_{\mu} - 1 = F_0\overline{\mathcal{K}}_\mu = F_0\overline{\mathcal{F}}, \tag{19b}$$

$$\Phi^{\mu}_{\rho} = F_0\overline{\mathcal{K}}'_\mu\frac{\partial\bar{\mu}}{\partial z} = F_0\overline{\mathcal{F}}'\frac{\partial\bar{\mu}}{\partial z}. \tag{19c}$$

Since $\Phi^{\rho}_{\rho} \geqslant 1$ and $\Phi^{\mu}_{\mu} \geqslant 1$ the integral on the left-hand side is nonnegative. The (real part of the) first term on the right-hand side, however, can have either sign, implying that the eigenvalue λ is not necessarily negative. This notion is the mathematical expression of the convective feedback (Welander, 1982; Lenderink and Haarsma, 1994). It may result in the occurrence of bifurcations, even when using $\mathcal{F}$ as convective adjustment function.

In the following we consider the case $i^{\mathrm{res}}_T = 1$ (relaxation of T) and $i^{\mathrm{res}}_S = 0$ (fixed salinity source), which most closely corresponds to the situation in the real ocean. An intuitive explanation of how the convective feedback causes multiple equilibria in this case was provided by Lenderink and Haarsma (1994): Given that the temperature forcing acts to destabilise the stratification, while the salinity forcing acts to stabilise it, convection may become self-sustaining due to the fact that it has a stronger neutralising impact on salinity than on temperature. If present, multiple equilibria are therefore expected for $\gamma < 0$ (stabilising salinity forcing), and would be associated with a reorganisation of the tracer distribution in the lower part of the column (where the temperature forcing is destabilising).

For the discretised model we can verify this prediction, but it turns out that the bifurcation diagram is not robust to changes in resolution. Using $F_0 = 10^2$ and $\epsilon = 10$ we perform two numerical experiments, one with $l = 10$ (equidistant) levels, and one with $l = 20$ levels. Branches of steady states are calculated using a pseudo-arclength continuation algorithm (Keller, 1977). The linear systems are solved using the matrix division operator implemented in MATLAB. The results are shown in Fig. 4. The vertical axes of the bifurcation diagrams show the sum of $\mathcal{F}(\partial_z\rho)$ across all interfaces, which is a measure of the range across which convection operates. For values of γ smaller than about -4×10^{-2} solutions exist with stable stratification throughout the column, i.e. $\sum\mathcal{F} = 0$. For values of γ larger than about 1 stratification is statically unstable in the entire column, i.e. $\sum\mathcal{F} = l-1$. The solutions on these two parts of the branch are linearly stable, while the part in between is characterised by a series of bifurcation points. For $\gamma > 0$ the bifurcations are Hopf bifurcations. Since we focus on the steady state dynamics, we have not quantitatively explored the intrinsic variability that originates from these singularities. For $\gamma < 0$ the bifurcations are saddle-nodes. When comparing the two experiments the most striking result is that the number of bifurcations is determined by the resolution. For $l = 10$ there are 6 pairs of back-to-back saddle-nodes, while there are 12 pairs for $l = 20$. In addition, the width of the region in parameter space where multiple equilibria exist decreases with increasing resolution.

Fig. 5 presents the profiles of density, temperature and salinity from the experiment with $l = 20$ for two values of γ close to zero. CA acts on that part of the column where the density gradient is positive, i.e. $z < -0.375$ for $\gamma = -0.01$ and $z < -0.325$ for $\gamma = 0.01$.

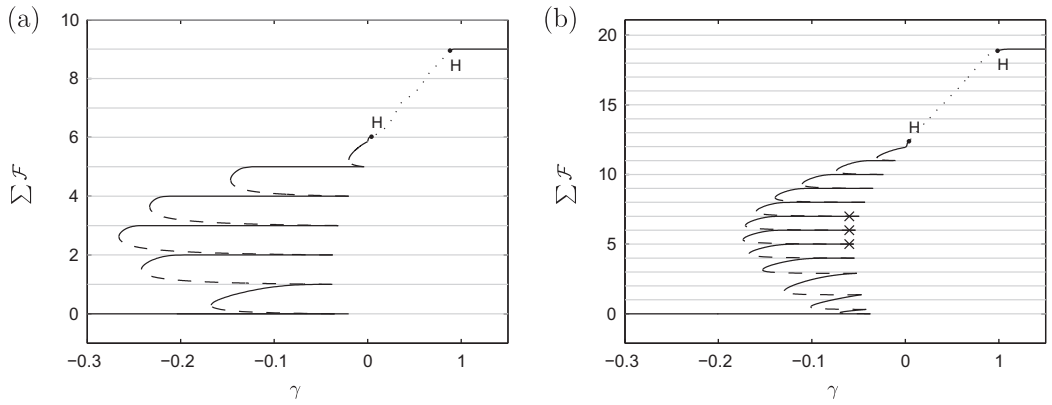

Fig. 4. Bifurcation diagrams for the one-dimensional model with traditional convective adjustment, using the salinity forcing strength γ as control parameter (note the variation in scale on the horizontal axis). Plotted is the sum of $\mathcal{F}(\partial_z \rho)$ across all interfaces for a vertical resolution of (a) 10 layers/9 interfaces and (b) 20 layers/19 interfaces. Drawing conventions are as in Fig. 1a. The crosses in (b) indicate the solutions shown in Fig. 6b.

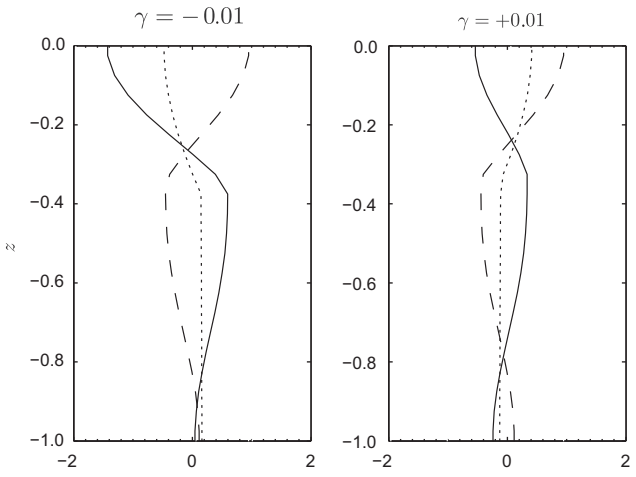

Fig. 5. Profiles of density (drawn), temperature (dashed) and salinity (dotted) from the experiment with $l = 20$ for two values of γ. The profiles for $\gamma = -0.01$ correspond to the solution with $\sum \mathcal{F} \approx 12$.

It is obvious that CA does not completely remove static instability: only in the limit $F_0 \to \infty$ the stratification becomes neutral. By virtue of the relatively small value of the convective efficiency ($F_0 = 10^2$) used here, the figure clearly illustrates the fact that CA has a much stronger impact on salinity than on temperature. It was explained above that multiple equilibria result from just this difference. For the discrete model it is clear, though, that the convective feedback mechanism operates on the grid scale, rather than independent of the discretisation. The resulting multiple steady states are therefore artificial.

From Eq. (19c) one may expect that if F_0 or $\overline{\mathcal{F}'}$ is made sufficiently small, no spurious bifurcations occur. Indeed, for $l = 10$, there are no bifurcations if $F_0 < 1.41 \times 10^{-2}$, while keeping $\epsilon = 10$, or if $\epsilon < 7.09 \times 10^{-2}$, while keeping $F_0 = 10^2$. In both cases CA would be completely ineffective. Furthermore, even if there are no bifurcations, the number of positive excursions of the least negative eigenvalue still depends on resolution (not shown). For the experiment with $l = 20$ the thresholds are only slightly larger: bifurcations disappear if $F_0 < 1.82 \times 10^{-2}$ or if $\epsilon < 8.14 \times 10^{-2}$.

3.4. Analytical approach

We have shown for the discrete case that the bifurcation behaviour that reflects the convective feedback, depends on resolution. Similar spurious behaviour was noted by V98 regarding the self-sustaining diffusion feedback, for which case a tentative explanation could be deduced from Eq. (17). In case of the convective feedback the explanation can be made more precise, because analytical steady solutions of Eq. (7) can be calculated, provided that the Heaviside step function is used as convective adjustment function for temperature and salinity,

$$\mathcal{K}_T = \mathcal{K}_S = \mathcal{H}\left(\frac{\partial \rho}{\partial z}\right). \tag{20}$$

As in the previous section, we use $F_0 = 10^2, i_T^{\mathrm{res}} = 1$ and $i_S^{\mathrm{res}} = 0$. We proceed by decoupling the intensity of convection from the stratification by introducing z_c, the shallowest level of convection, and substituting

$$\mathcal{H}\left(\frac{\partial \rho}{\partial z}\right) \to \mathcal{H}(z_c - z) \tag{21}$$

in Eq. (7). The implication is that the diffusivity equals 1 for $z > z_c$ and $1 + F_0$ for $z < z_c$. The next step is to solve the diffusion equations for both parts of the domain and to match them afterwards. The complete solution is rather lengthy and therefore presented in the Appendix. By combining the results for T and S the analysis gives a solution $\rho = \rho(z, z_c, \gamma)$. Now we consider the function $\partial_z \rho(z, z_c, \gamma)$ and try to find z_c such that it is positive for $z < z_c$ and negative for $z > z_c$, because only then is the substitution defined by Eq. (21) appropriate. In the following, such values of z_c are referred to as "consistent".

Fig. 6a demonstrates that consistent values of z_c exist for all values of γ, except for a window between 0.024 and 0.800. It should be noted that a solution is linearly stable for a fixed value of z_c, because the governing equations are linear. A proper analysis of the stability properties of this system would hence require considering perturbations in z_c, which turns out to be tedious. The stability indicated in Fig. 6a is therefore simply inferred from the fact that a change in linear stability is a generic feature of a saddle-node bifurcation. The main result of this exercise is that there is only a single pair of saddle-node bifurcations in the continuous model. These represent the "true" expression of convective feedback in the column model.

When treating this problem numerically, there are two fundamental limitations that cause multiple equilibria due to CA to be artificial. The first limitation is that z_c may only be taken from a finite discrete set of values. Mesh size convergence is only achieved if z_c equals one of the levels z_k at which the discrete tracers are calculated. For the l-point equidistant grid used in the analysis above these are given by

$$z_k = \frac{1}{l}\left(k - l - \frac{1}{2}\right) \quad k = 1, \ldots, l. \tag{22}$$

In general, the consistent value of z_c will not coincide with any z_k.

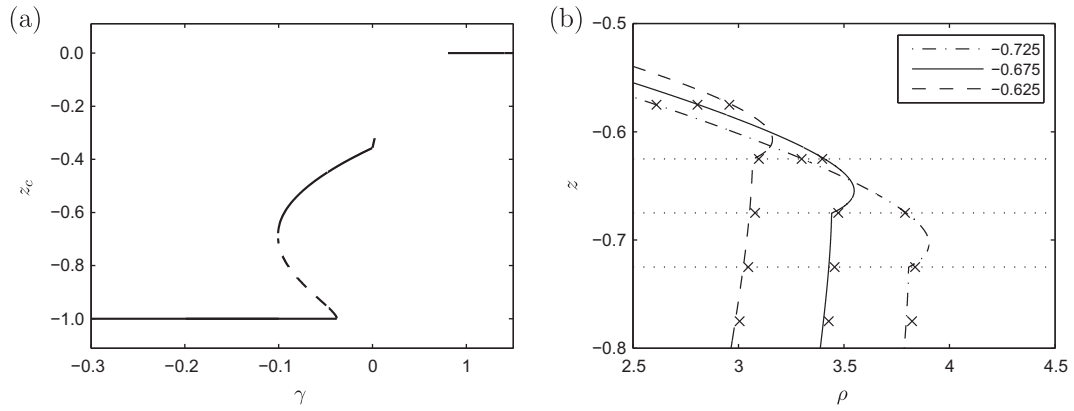

Fig. 6. (a) Bifurcation diagram showing the consistent value of z_c for the analytical solution to the one-dimensional model with traditional convection. There are no consistent solutions within the interval $\gamma \in (0.024, 0.800)$. (b) Analytic density profiles for $\gamma = -0.06$, using three *inconsistent* values of z_c (indicated by horizontal dotted lines), and corresponding numerical solutions (crosses) from the experiment with $l = 20$.

As an example we consider $\gamma = -0.06$, in which case the consistent $z_c = -0.478$ for the convecting, linearly stable solution (Fig. 6a). In the experiment with $l = 20$ (Fig. 4b) 23 solutions were found for $\gamma = -0.06$ (of which 12 are linearly stable); here we focus on the three linearly stable solutions with $\sum \mathcal{F} \approx 5$, $\sum \mathcal{F} \approx 6$, and $\sum \mathcal{F} \approx 7$, respectively. In these cases the discrete density gradients are such that at each interface $\mathcal{F}(l[\rho_{k+1} - \rho_k])$ is either 0 or 1 (due to finite computational precision), which implies that $\mathcal{F}$ could be replaced by $\mathcal{H}$ without changing the solution. In other words, the numerical solutions we examine might as well have been obtained using $\mathcal{H}$. We may also consider them as solutions of the problem in which the diffusivity is prescribed as $1 + F_0\mathcal{H}(z_c - z)$, where $z_c = -0.725$, $z_c = -0.675$ and $z_c = -0.625$, respectively. So, in each case the value of z_c is inconsistent in the continuous case. We would therefore not like these numerical solutions, which are good approximations of the corresponding inconsistent analytical solutions (Fig. 6b), to exist.

Numerical solutions with inconsistent values of z_c nonetheless appear as viable solutions, which is due to the second limitation involved in the discretisation of the problem: As demonstrated in Fig. 6b, the density gradients needed to evaluate $\mathcal{H}(\partial_z\rho)$ are not adequately resolved. The discrete derivative across the interval above $z = z_c$ is an average that does not capture the positive density gradient present in the analytical solution. In the contrary, the numerical gradient is of opposite sign. The solution is hence falsely considered consistent, which explains its existence. The multiple equilibria of the discrete model are thus completely artificial, both if $\mathcal{F}$ is used, as in subsection 3.3 (Fig. 4), as well as if $\mathcal{H}$ is used, as in conventional ocean models. Note, though, that only in the former case the spurious multiple steady states are connected through branches of linearly unstable solutions.

Increasing the resolution might seem to mitigate the problem, as such would improve the discrete estimates of continuous derivatives. Indeed, it leads to a reduction in the range of γ across which the spurious solutions are possible. Our results suggest, however, that the correct linear stability properties are only found in the continuous limit. This would imply that the convective feedback cannot be captured by a discrete model that uses CA.

4. Eliminating the spurious multiple equilibria

In the previous section we established that the numerous multiple equilibria associated with CA arise due to a model artifact. Although we believe this to be a fundamental problem, in this section we seek to establish a pragmatic remedy: the aim is to be able to apply a form of CA without severely diminishing the effectiveness of implicit modelling. Two alternative CA formulations are proposed in which the spurious model behaviour is eliminated, or at least reduced. The new schemes result from modifications to the traditional CA scheme that are motivated by the results of the previous section. By implementing the alternative formulations in the two-dimensional model of Section 2 we assess the impact they have on the large-scale dynamical behaviour.

4.1. Density mixing

We first investigate a scheme in which multiple equilibria are absent by definition. It was shown in Section 3.3 that positive eigenvalues are caused by the interaction of density and spiciness gradients. This interaction can be eliminated by choosing

$$\mathcal{K}_\rho = \mathcal{F}\left(\frac{\partial\rho}{\partial z}\right), \quad \mathcal{K}_\mu = 0, \tag{23}$$

in which case Eq. (19b) and (19c) would change to $\Phi^\mu_\mu = 1$ and $\Phi^\mu_\rho = 0$. As a result, the eigenvalues λ of the one-dimensional column model are always negative [Eq. (18)]. Qualitatively, this formulation implies that density is affected by convection, while spiciness is not. This approach is therefore called "density mixing". We repeat the $l = 20$ experiment of Section 3.3 to find that the resulting solution branch is indeed free of bifurcations (Fig. 7a). The spurious additional multiple equilibria introduced by traditional CA also disappear from the two-dimensional model results (Fig. 7b). Yet, the two pitchfork bifurcations, which are the signature of the large-scale salt advection feedback, are maintained. It is even possible to create the bifurcation diagram for very efficient convection, $F_0 = 10^5$, without running into computational problems.

However, these benefits come at a cost. The main disadvantage of this scheme is most easily illustrated by the equations for temperature and salinity in the one-dimensional model, which are given by

$$\frac{\partial T}{\partial t} = \frac{1}{P}\frac{\partial^2 T}{\partial z^2} + \frac{F_0}{2P}\frac{\partial}{\partial z}\left(\mathcal{F}\left(\frac{\partial\rho}{\partial z}\right)\cdot\left[\frac{\partial T}{\partial z} - \frac{\partial S}{\partial z}\right]\right) - \left(i_T^{\mathrm{res}}T - \widetilde{T}(z)\right), \tag{24a}$$

$$\frac{\partial S}{\partial t} = \frac{1}{P}\frac{\partial^2 S}{\partial z^2} + \frac{F_0}{2P}\frac{\partial}{\partial z}\left(\mathcal{F}\left(\frac{\partial\rho}{\partial z}\right)\cdot\left[\frac{\partial S}{\partial z} - \frac{\partial T}{\partial z}\right]\right) - \left(i_S^{\mathrm{res}}S - \widetilde{S}(z)\right). \tag{24b}$$

It is clear that gradients in a tracer are created due to density mixing, even if that tracer is unforced. For example, if $\widetilde{S}(z) = 0$, the solution of Eq. (24b) is different from $S(z) = 0$. Fig. 8, which may be compared to Fig. 5, illustrates this point for $i_T^{\mathrm{res}} = 1$, $i_S^{\mathrm{res}} = 0$. In com-

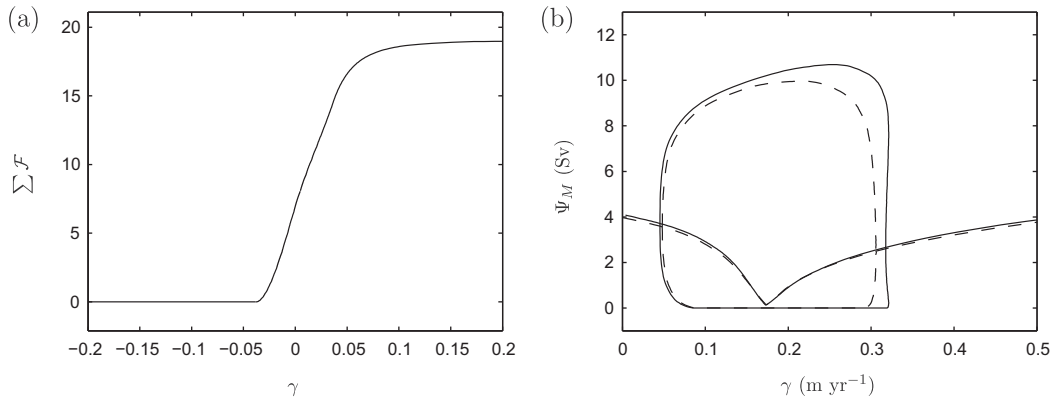

Fig. 7. Bifurcation diagram for the (a) one-dimensional and (b) two-dimensional model with density mixing. In (b) linear stability is not indicated; the solid line corresponds to $F_0 = 10^2$ and the dashed line to $F_0 = 10^5$.

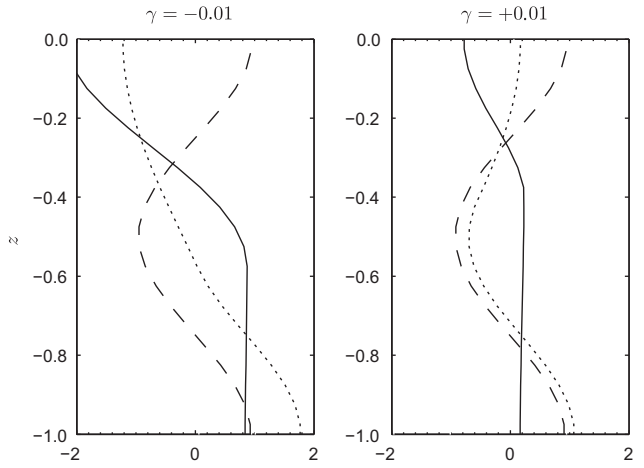

Fig. 8. Same as Fig. 5, but for density mixing.

parison to the traditional formulation the (positive) density gradient in the part of the column with active CA is rather weak, which is achieved by mutual compensation of temperature and salinity gradients, i.e. $\partial_z T \approx \partial_z S \approx \partial_z \mu/2$. The specified forcing allows salinity to be affected much stronger by CA than temperature. The creation of gradients due to density mixing is thus most apparent in the salinity profile.

4.2. Conditional mixing

The second alternative formulation is based on a partial disruption of the feedback that causes the multiple equilibria. By choosing the convective adjustment function for temperature and salinity as

$$\mathcal{K}_T = \mathcal{F}\left(\frac{\partial \rho}{\partial z}\right) \cdot \mathcal{F}\left(-\frac{\partial T}{\partial z}\right), \quad \mathcal{K}_S = \mathcal{F}\left(\frac{\partial \rho}{\partial z}\right) \cdot \mathcal{F}\left(\frac{\partial S}{\partial z}\right), \tag{25}$$

convection only operates on a tracer if both the tracer and the density stratification are statically unstable. This approach is therefore coined "conditional mixing". Unlike density mixing, this form of CA cannot by itself generate a gradient in a tracer profile. In the one-dimensional experiment of Section 3.3 the salinity stratification is statically stable across the entire depth range for $\gamma < 0$. Conditional mixing then results in $\mathcal{K}_S = 0$, which implies that convection cannot become self-sustaining. For $\gamma > 0$ the region of convection expands across the upper part of the domain, where temperature is stably stratified and thus unaffected by CA. There is hence also no interaction between temperature and salinity for positive salinity forcing. Fig. 9a shows that the bifurcation diagram is indeed free of bifurcations, while Fig. 10 illustrates how conditional mixing affects the tracer profiles.

If the forcing or model parameters are modified, however, the absence of singularities cannot be guaranteed. Applying the analysis demonstrated in Section 3.2 leads to

$$\int_{-1}^{0} \left(\frac{\Upsilon_T^T}{P} \frac{\partial \widehat{\Delta T}}{\partial z} \frac{\partial \Delta T}{\partial z} + i_T^{\text{res}} |\Delta T|^2 \right) \mathrm{d}z = - \int_{-1}^{0} \left(\frac{\Upsilon_S^T}{P} \frac{\partial \widehat{\Delta T}}{\partial z} \frac{\partial \Delta S}{\partial z} + \lambda |\Delta T|^2 \right) \mathrm{d}z \tag{26}$$

for the temperature equation [Eq. (7a)] and to

$$\int_{-1}^{0} \left(\frac{\Upsilon_S^S}{P} \frac{\partial \widehat{\Delta S}}{\partial z} \frac{\partial \Delta S}{\partial z} + i_S^{\text{res}} |\Delta S|^2 \right) \mathrm{d}z = - \int_{-1}^{0} \left(\frac{\Upsilon_T^S}{P} \frac{\partial \widehat{\Delta S}}{\partial z} \frac{\partial \Delta T}{\partial z} + \lambda |\Delta S|^2 \right) \mathrm{d}z \tag{27}$$

for the salinity equation [Eq. (7b)], where we used the following definitions:

$$\Upsilon_T^T = 1 - F_0 \mathcal{F}'(\partial_z \bar{\rho}) \mathcal{F}(-\partial_z \overline{T}) \partial_z \overline{T} + F_0 \mathcal{F}(\partial_z \bar{\rho}) (\mathcal{F}(-\partial_z \overline{T}) - \mathcal{F}'(-\partial_z \overline{T}) \partial_z \overline{T}), \tag{28a}$$

$$\Upsilon_S^S = 1 + F_0 \mathcal{F}'(\partial_z \bar{\rho}) \mathcal{F}(\partial_z \overline{S}) \partial_z \overline{S} + F_0 \mathcal{F}(\partial_z \bar{\rho}) (\mathcal{F}(\partial_z \overline{S}) + \mathcal{F}'(\partial_z \overline{S}) \partial_z \overline{S}), \tag{28b}$$

$$\Upsilon_S^T = F_0 \mathcal{F}'(\partial_z \bar{\rho}) \mathcal{F}(-\partial_z \overline{T}) \partial_z \overline{T}, \tag{28c}$$

$$\Upsilon_T^S = -F_0 \mathcal{F}'(\partial_z \bar{\rho}) \mathcal{F}(\partial_z \overline{S}) \partial_z \overline{S}. \tag{28d}$$

Because $\Upsilon_T^T \geqslant 0$ the integral on the left-hand side of Eq. (26) is always nonnegative. So, this relation only allows eigenvalues to be nonnegative if $\Delta T = 0$ or if $\Upsilon_S^T \partial_z \Delta S$ is nonzero for some range $z \in Z_T$. If the first condition holds, Eq. (27) implies $\lambda < -i_S^{\text{res}}$, because $\Upsilon_S^S \geqslant 0$. So nonnegative eigenvalues are only possible if the second condition is satisfied. Hence, ΔS must be nonzero, which through Eq. (27) leads to the condition that Υ_T^S must be nonzero for some range $z \in Z_S$. In summary, for eigenvalues to be nonnegative it is required that Υ_S^T is nonzero for some $z \in Z_T$ *and* that Υ_T^S is nonzero for some $z \in Z_S$, where Z_T and Z_S are not empty. This condition is more restrictive than that for traditional CA, in which case $\overline{\mathcal{F}'} \partial_z \bar{\mu}$ must be nonzero for nonnegative eigenvalues to be possible. Nonetheless, although the condition is not satisfied for any γ in the problem of Section 3.3, it may well be in general, as illustrated by the two-dimensional model results.

As with density mixing, the two-dimensional model operates without computational difficulties, even for $F_0 = 10^5$. In addition, the bifurcation diagram (Fig. 9b) shows that the large-scale

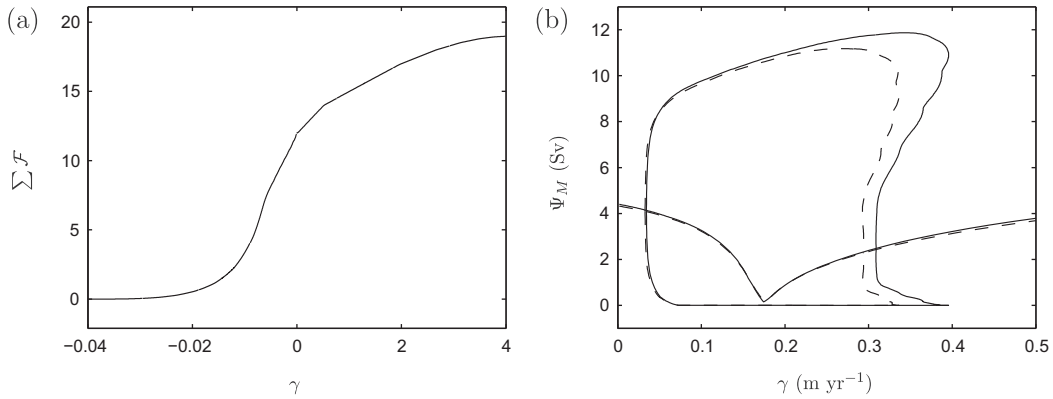

Fig. 9. Same as Fig. 7, but for conditional mixing. Note the variation in scale on the horizontal axis of the plot in panel a.

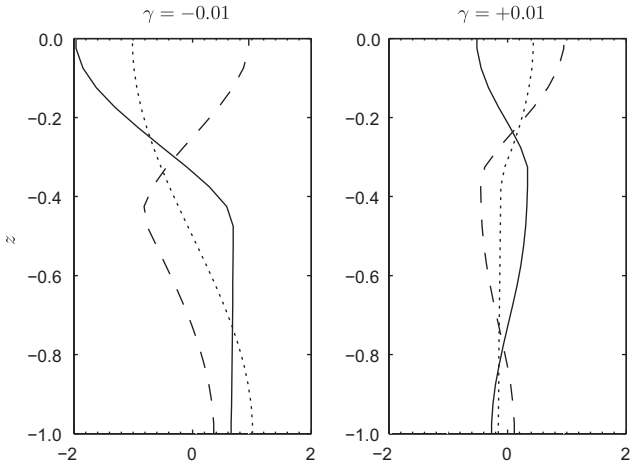

Fig. 10. Same as Figs. 5 and 8, but for conditional mixing.

dynamics are not affected qualitatively by conditional mixing. Different from the density mixing case, saddle-node bifurcations occur along the branches of the equatorially asymmetric solutions, but only on the parts where γ is larger than about 0.28 m yr^{-1}. Compared to traditional CA there are clearly less singularities, and those that are present do not raise computational problems.

5. Summary and discussion

In this paper we reexamined the origin of the multiple equilibria in ocean-climate models that arise due to convective adjustment. Their occurrence presents a challenge to the application of numerical bifurcation analysis in these models. The problem was first illustrated in a fully-implicit two-dimensional primitive equation model. By varying the strength of the surface virtual salt flux a multitude of saddle-node bifurcations was shown to occur (Fig. 2a). Next, the cause of these bifurcations was analysed in detail using the one-dimensional column model introduced by V98, but extended in this study to include both temperature and salinity. A regime of multiple equilibria was identified and it was demonstrated that the number of coexisting steady states increases with increasing resolution, while the extent of the parameter space in which they occur decreases (Fig. 4). By comparing numerical and analytical results we showed that the multiple equilibria are inherent to discretisation of CA and therefore artificial (Fig. 6b). Finally, we proposed two alternative formulations of CA and demonstrated that these can be used as a pragmatic solution to the difficulty of applying CA in implicit models.

It should be emphasised that the extension of the column model of V98 to include two tracers is necessary to fully understand the problem of artificial multiple equilibria. By analytically establishing the conditions required for the existence of zero eigenvalues of the Jacobian matrix (which implies bifurcations), we found two different feedback mechanisms that may be responsible for multiple equilibria. V98 only captured the feedback of self-sustaining diffusion, which may occur if there is sub-critical mixing for weakly stable stratification. We eliminated this mechanism by choosing a convective adjustment function in which there is no sub-critical mixing. This allowed us to focus on the nonlinear interaction of density and spiciness gradients that occurs due to the asymmetry in temperature (damping) and salinity (no damping) forcing. The associated feedback mechanism was discussed before by Lenderink and Haarsma (1994) and is also present in the simple box model of Welander (1982). In contrast to these studies, our results indicate that there is no meaningful way to capture this feedback in a discrete model by using CA, despite its possible relevance in the real world.

Our results suggest a close correspondence between the behaviour of CA in the two-dimensional model and the column model. For example, we demonstrated analytically that multiple equilibria can be eliminated from the column model by density mixing, and showed numerically that also no spurious saddle-nodes occur due to CA when using this scheme in the two-dimensional model. This strongly suggests that the additional multiple equilibria in the two-dimensional model with traditional convection are solely due to the parameterisation and are not induced by a response of resolved processes on changes in density caused by CA.

Still, it should be kept in mind that the one-dimensional model cannot be perceived as representing a column from a full ocean model. Rather, it allows to evaluate the properties of CA in a controlled way. We specifically note that the forcing was distributed along the entire column, instead of specified as boundary conditions at the top. In the latter case, the forcing would also have influenced the temperature and salinity across the full depth range, but only in an uncontrolled manner. Furthermore, conditions in the ocean model may correspond to other parameter values and forcing functions than used in the above, which were merely chosen such as to clearly illustrate the problems of CA.

The asset of the coarse-resolution (non eddy-permitting) modelling approach is that it allows to study the dynamical processes that might become obscured when as a result of higher resolution simulations on centennial to millennial timescales become computationally inaccessible. We believe that the relevance of the alternative CA formulations presented in Section 4 should be assessed

from this point of view. Both schemes help to realise a density field that respects the physical requirement that no static instabilities should be present at large spatial or temporal scales. At the same time they facilitate the use of numerical continuation techniques in coarse-resolution ocean models by avoiding (density mixing) or reducing (conditional mixing) the occurrence of artificial multiple equilibria.

The alternative schemes are not meant to faithfully reproduce the water mass characteristics seen in convective areas in the ocean – although the performance of traditional CA is probably not superior in this respect. Therefore no attempt was made to compare the action of these schemes with data or high-resolution model output. It should be noted, though, that the fact that traditional, density and conditional mixing produce different temperature and salinity profiles, implies that large-scale dynamics are affected differently by these schemes. In the context of the two-dimensional model, this is clear from comparison of the (overall) bifurcation structure presented in Figs. 2a, 7b, and 9b. It is not straightforward to explain exactly how any of the different forms of CA deforms a bifurcation diagram. The bifurcation behaviour due to the salt advection feedback (Stommel, 1961), however, is qualitatively the same for different CA schemes.

It remains to be explored if this robustness transfers to three-dimensional models, since flow dynamics are severely altered between the two- and three-dimensional case (Rahmstorf, 1995). Yet, it turns out that, compared to computations without CA, applying the Newton–Raphson method to a model with one of the alternative CA schemes of Section 4 still produces rather ill-posed systems, even if the artificial bifurcations due to traditional CA are absent or reduced in number. As a result, exploring the three-dimensional case is currently too challenging from a computational point of view. The technical details of this problem are beyond the scope of this paper, but there are good prospects of resolving the issue. A hint of what might be expected if the flow dynamics were three-dimensional is provided by Weijer and Dijkstra (2001). They showed that the bifurcation diagram for the two-dimensional model is qualitatively similar to that of its three-dimensional extension, which was obtained by consecutively adding Earth rotation and surface wind stress. No CA was applied, however, so this result corresponds to the case with unstable stratification present in high latitudes. Nonetheless, using an iterative post-processing procedure, which avoids the problems of using CA in a numerical continuation experiment, Weijer and Dijkstra (2001) found that the mechanism of symmetry-breaking is probably not affected by the convective adjustment procedure. It may therefore well be that the alternatives presented in Section 4 also mitigate the problems of applying CA in more complete models without affecting the relevant large-scale feedbacks.

Throughout this paper, we have focussed on the use of numerical bifurcation techniques. It is to be emphasised, however, that artificial multiple steady states due to CA also occur in time-stepping models that are run until equilibrium is reached. Although the multiplicity was not classified as artificial behaviour, Rahmstorf (1995) showed that in his idealised three-dimensional model many different convection patterns were stable under the same boundary conditions, using finite amplitude perturbations to switch between these states. Yet, it should be stated that the spurious saddle-node bifurcations due to CA are not evident in the hysteresis behaviour of all ocean models (e.g. Sijp et al., 2006). Most likely, this is because a hysteresis experiment is inherently transient and can only result in approximate bifurcation diagrams. Even if the anomalous freshwater forcing is increased sufficiently slowly in time, the artificial steady states due to CA are not easily recognised, because the "jump" from one state to the other is relatively small (at least when overturning rate is used as measure of the solution, Fig. 2). It is however also possible that the artificial saddle-node bifurcations are not as ubiquitous as in the two-dimensional model results of Section 2, because convection is more limited in space. Unlike the implicit model used here, most time-stepping codes currently employ isoneutral Redi (1982) and Gent and McWilliams (1990) mixing of tracers instead of simple horizontal diffusion. In a comparison of the two tracer mixing schemes Danabasoglu et al. (1994) showed that the use of the former causes convection to become much less widespread. Sijp et al. (2006) and Sijp and England (2009) suggested that this reduction is mainly due to isoneutral mixing and its interaction with the surface boundary conditions.

Eventually, computational resources will be no longer a limiting factor to run global simulations of the ocean at a resolution sufficient to capture the convective instability. This notwithstanding, coarser models probably remain valuable tools, provided that sub-grid scale motions such as convection are parameterised in a way that is acceptable for the problem under study. Our results, in conjunction with previous work (Cessi, 1996; Cessi and Young, 1996; Vellinga, 1998; Hughes et al., 2009), demonstrate that convective adjustment has serious deficiencies. This strongly motivates to continue the development of parameterisations of convection that are both physically sound, and can be implemented in a numerical model without introducing artificial dynamics.

Acknowledgements

This work was supported by the Netherlands Organisation for Scientific Research (NWO) through a Toptalent grant to MdT. The authors would like to thank both anonymous referees for their helpful comments on the manuscript

Appendix A. The analytical solution

Under the conditions specified in Section 3.4, and defining $Q = P(1 + F_0)^{-1}$, the temperature satisfies

$$0 = \frac{1}{Q}\frac{\partial^2 T}{\partial z^2} - T + \cos(2\pi z) \quad \text{for } z < z_c, \tag{A.1a}$$

$$0 = \frac{1}{P}\frac{\partial^2 T}{\partial z^2} - T + \cos(2\pi z) \quad \text{for } z > z_c. \tag{A.1b}$$

We require that the temperature and the diffusive temperature flux are continuous across $z = z_c$ and obtain

$$T = A_1 \cos(2\pi z) + B_1 \cosh\left(\sqrt{Q}(z+1)\right) \quad \text{for } z < z_c, \tag{A.2a}$$

$$T = A_2 \cos(2\pi z) + B_2 \cosh\left(\sqrt{P}z\right) \quad \text{for } z > z_c. \tag{A.2b}$$

Here,

$$A_1 = \left(1 + \frac{4\pi^2}{Q}\right)^{-1}, \tag{A.3a}$$

$$A_2 = \left(1 + \frac{4\pi^2}{P}\right)^{-1}, \tag{A.3b}$$

$$B_1 \cosh\left(\sqrt{Q}(z_c+1)\right) = \frac{2\pi\left(\frac{P}{Q}A_1 - A_2\right)\sin(2\pi z_c) + (A_1 - A_2)\cos(2\pi z_c)\sqrt{P}\tanh\left(\sqrt{P}z_c\right)}{\frac{P}{Q}\sqrt{Q}\tanh\left(\sqrt{Q}(z_c+1)\right) - \sqrt{P}\tanh\left(\sqrt{P}z_c\right)}, \tag{A.3c}$$

$$B_2 \cosh\left(\sqrt{P}z_c\right) = \frac{2\pi\left(\frac{P}{Q}A_1 - A_2\right)\sin(2\pi z_c) + (A_1 - A_2)\cos(2\pi z_c)\frac{P}{Q}\sqrt{Q}\tanh\left(\sqrt{Q}(z_c+1)\right)}{\frac{P}{Q}\sqrt{Q}\tanh\left(\sqrt{Q}(z_c+1)\right) - \sqrt{P}\tanh\left(\sqrt{P}z_c\right)}. \tag{A.3d}$$

The salinity profile is determined from

$$0 = \frac{1}{Q}\frac{\partial^2 S}{\partial z^2} + \gamma\cos(\pi z) \quad \text{for } z < z_c, \tag{A.4a}$$

$$0 = \frac{1}{P}\frac{\partial^2 S}{\partial z^2} + \gamma\cos(\pi z) \quad \text{for } z > z_c. \tag{A.4b}$$

We impose continuity of S at $z = z_c$ and the integral constraint

$$\int_{-1}^{0} S\mathrm{d}z = 0$$

to find

$$\gamma^{-1}S = C_1\cos(\pi z) + D_1 \quad \text{for } z < z_c, \tag{A.5a}$$

$$\gamma^{-1}S = C_2\cos(\pi z) + D_2 \quad \text{for } z > z_c, \tag{A.5b}$$

where

$$C_1 = \frac{Q}{\pi^2}, \tag{A.6a}$$

$$C_2 = \frac{P}{\pi^2}, \tag{A.6b}$$

$$D_1 = \frac{P-Q}{\pi^3}(\sin(\pi z_c) - \pi z_c\cos(\pi z_c)), \tag{A.6c}$$

$$D_2 = \frac{P-Q}{\pi^3}(\sin(\pi z_c) - \pi(z_c+1)\cos(\pi z_c)). \tag{A.6d}$$

References

Cessi, P., 1996. Grid-scale instability of convective-adjustment schemes. Journal of Marine Research 54, 407–420.

Cessi, P., Young, W.R., 1996. Some unexpected consequences of the interaction between convective adjustment and horizontal diffusion. Physica D: Nonlinear Phenomena 98, 287–300.

Clark, P.U., Pisias, N.G., Stocker, T.F., Weaver, A.J., 2002. The role of the thermohaline circulation in abrupt climate change. Nature 415, 863–869.

Danabasoglu, G., McWilliams, J.C., Gent, P.R., 1994. The role of mesoscale tracer transports in the global ocean circulation. Science 264, 1123–1126.

De Niet, A., Wubs, F., Terwisscha van Scheltinga, A., Dijkstra, H.A., 2007. A tailored solver for bifurcation analysis of ocean-climate models. Journal of Computational Physics 227, 654–679.

Dijkstra, H.A., Ghil, M., 2005. Low-frequency variability of the large-scale ocean circulation: a dynamical systems approach. Reviews of Geophysics 43, RG3002.

Flament, P., 2002. A state variable for characterizing water masses and their diffusive stability: spiciness. Progress in Oceanography 54, 493–501.

Gent, P.R., McWilliams, J.C., 1990. Isopycnal mixing in ocean general circulation models. Journal of Physical Oceanography 20, 150–155.

Hughes, G.O., Hogg, A.M.C., Griffiths, R.W., 2009. Available potential energy and irreversible mixing in the meridional overturning circulation. Journal of Physical Oceanography 39, 3130–3146.

Jones, H.J., Marshall, J., 1993. Convection with rotation in a neutral ocean: a study of open ocean deep convection. Journal of Physical Oceanography 23, 1009–1039.

Keller, H.B., 1977. Numerical solution of bifurcation and nonlinear eigenvalue problems. In: Rabinowitz, P.H. (Ed.), Applications of Bifurcation Theory. Academic Press, New York, USA.

Lenderink, G., Haarsma, H., 1994. Variability and multiple equilibria of the thermohaline circulation associated with deep-water formation. Journal of Physical Oceanography 24, 1480–1493.

Marotzke, J., 1991. Influence of convective adjustment on the stability of the thermohaline circulation. Journal of Physical Oceanography 21, 903–907.

Marotzke, J., Scott, J.R., 1999. Convective mixing and the thermohaline circulation. Journal of Physical Oceanography 29, 2962–2970.

Marotzke, J., Willebrand, J., 1991. Multiple equilibria of the global thermohaline circulation. Journal of Physical Oceanography 21, 1372–1385.

Meehl, G., Stocker, T., Collins, W., Friedlingstein, P., Gaye, A., Gregory, J., Kitoh, A., Knutti, R., Murphy, J., Noda, A., Raper, S., Watterson, I., Weaver, A.J., Zhao, Z.C., 2007. Global climate projections. In: Solomon, S., Qin, D., Manning, M., Chen, Z., Marquis, M., Averyt, K.B., Tignor, M., Miller, H.L. (Eds.), Climate Change 2007: The Physical Science Basis. Contribution of Working Group I to the Fourth Assessment Report of the Intergovernmental Panel on Climate Change. Cambridge University Press, Cambridge, United Kingdom and New York, NY, USA.

Rahmstorf, S., 1995. Multiple convection patterns and thermohaline flow in an idealized ogcm. Journal of Climate 8, 3028–3039.

Rahmstorf, S., 1999. Rapid transitions of the thermohaline ocean circulation – a modelling perspective. In: Abrantes, F., Mix, A.C. (Eds.), Reconstructing Ocean History: A Window into the Future. Kluwer Academic/Plenum Publisher, pp. 139–149.

Rahmstorf, S., Crucifix, M., Ganopolski, A., Goosse, H., Kamenkovich, I., Knutti, R., Lohmann, G., Marsh, R., Mysak, L.A., Wang, Z., Weaver, A.J., 2005. Thermohaline circulation hysteresis: a model intercomparison. Geophysical Research Letters 32.

Redi, M.H., 1982. Oceanic isopycnal mixing by coordinate rotation. Journal of Physical Oceanography 12, 1154–1158.

Schmidt, G.A., Mysak, L.A., 1996. The stability of a zonally averaged thermohaline circulation model. Tellus 48A, 158–178.

Seydel, R., 1988. From Equilibrium to Chaos – Practical Bifurcation and Stability Analysis. Elsevier Science. 367pp.

Sijp, W.P., England, M.H., 2009. The control of polar haloclines by along-isopycnal diffusion in climate models. Journal of Climate 22, 486–498.

Sijp, W.P., Bates, M., England, M.H., 2006. Can isopycnal mixing control the stability of the thermohaline circulation in ocean climate models? Journal of Climate 19, 5637–5651.

Sleijpen, G.L.G., Van der Vorst, H.A., 1996. A Jacobi–Davidson iteration method for linear eigenvalue problems. SIAM Journal on Matrix Analysis and Application 17, 401–425.

Stommel, H., 1961. Thermohaline convection with two stable regimes of flow. Tellus 13, 224–230.

Vellinga, M., 1997. Bifurcations and dynamics of the ocean's thermohaline circulation. Ph.D. Thesis, Utrecht University (Available from Institute for Marine and Atmospheric research Utrecht, Utrecht University, Princetonplein 5, 3584 CC Utrecht, The Netherlands).

Vellinga, M., 1998. Multiple equilibria in ocean models as a side effect of convective adjustment. Journal of Physical Oceanography 28, 621–633.

Weijer, W., Dijkstra, H.A., 2001. A bifurcation study of the three-dimensional thermohaline ocean circulation: the double hemispheric case. Journal of Marine Research 59, 599–631.

Welander, P., 1982. A simple heat-salt oscillator. Dynamics of Atmospheres and Oceans 6, 233–242.